OPEN ACCESS
Journal of Multidisciplinary Applied Natural Science Vol. 6 No. 3 (2026) https://doi.org/10.47352/jmans.2774-3047.383
Check for updates
Research Article

Synthesis, Structural, Spectroscopic, and DFT Characterization of a Thermodynamically Stable Bis (quercetin)copper(II) Complex and Its α-Amylase Inhibitory Activity

Puteri Khansa Salsabila, Yusi Deawati, Regaputra Satria Janitra, Safri Ishmayana, Iman Permana Maksum, Yessi Permana, and Yudha Prawira Budiman*

Received : January 23, 2026	Revised : March 27, 2026	Accepted : April 3, 2026	Online : May 6, 2026

Abstract
Quercetin (Q) is a dietary flavonol with promising antidiabetic activity but limited therapeutic utility due to poor solubility and low bioavailability. Herein, we report a temperature-controlled synthesis, structural characterization, and α-amylase inhibitory activity of a copper(II)–quercetin (CuQ) complex prepared from a 1:1 Cu(II):quercetin mixture in methanol at 65 °C. The characterization techniques include an elemental analysis (EA), AAS, TGA, MSB, UV-Vis, and FTIR. Elevated temperature predominantly affords a bis(quercetin)-Cu(II) complex, $[Cu(H_2O)(Q)_2]\cdot 4H_2O$, supported by DFT calculations. Spectroscopic, thermal, and magnetic data are consistent with a proposed mononuclear Cu(II) structure, in which the metal center is coordinated by two quercetin ligands. DFT calculations suggest a thermodynamic preference for the complex, with the relative reaction free energy ($\Delta\Delta G^{o}_{reaction}$ = 32.93 kcal mol^{-1}) representing the difference in Gibbs free energy change between the formation of CuQ 1:1 and 1:2 complexes, confirming the higher stability of CuQ 1:2. The complex exhibits enhanced α-amylase inhibitory activity (IC_{50} = 133 µM) compared to free quercetin (IC_{50} = 450 µM). The apparent IC_{50} value is reported alongside acarbose (IC_{50} = 148 µM) under identical assay conditions. These findings indicate that the coordination of Q with Cu(II) enhances the inhibitory activity of the α-amylase enzyme.

Keywords: α-amylase, copper, DFT, metal-flavonoid complex, quercetin

1. INTRODUCTION

Quercetin (Q) or 2-(3,4-dihydroxyphenyl)-3,5,7-trihydroxy-4*H*-chromen-4-one is one of the most common and well-studied flavonols [1]–[3], widely found in fruits and vegetables [2]. Q exhibits diverse pharmacological activities, including antioxidant, antidiabetic, anti-inflammatory, antimicrobial, anti-osteoporotic, and anticancer effects [1][4]. In glucose homeostasis models, Q supports β-cell regeneration and insulin secretion, thereby improving glycemic control in chemically induced diabetes [5]. Consistent with these antidiabetic actions, Q inhibits human pancreatic α-amylase *in vitro* [6]. It also inhibits α-amylase and α -glucosidase, thereby reducing postprandial glucose excursions [7].

Despite these promising activities, the therapeutic application of Q is limited by poor aqueous solubility [8], pronounced hydrophobicity, low chemical stability, and low bioavailability, which collectively reduce its gastrointestinal absorption and systemic exposure [4][5][7][9]. Metal-ion complexation is widely used as a strategy to improve solubility and bioavailability of Q relative to its free form, thereby enhancing its pharmacological performance [9][10]. This strategy is supported by the presence of multiple oxygen-donor sites in Q, enabling coordination with various metal ions [11]. Three coordination domains are most frequently implicated (Figure 1): the B-ring catechol (3′,4′-dihydroxyl), the C-ring 3-OH/4-oxo site, and the 5-OH/4-oxo site [11]–[13]. These features make Q a versatile metal chelator [12][13].

Among the first-row transition-metal–quercetin systems, copper–quercetin complexes exhibit relatively high stability under comparable experimental conditions [1][11][14]. Complexation with Cu(II) is also chemically consequential because it can reshape the redox behavior of the flavonoid. Previous studies report enhanced radical-scavenging performance (DPPH/ABTS) and reduced ROS generation in copper-catalyzed

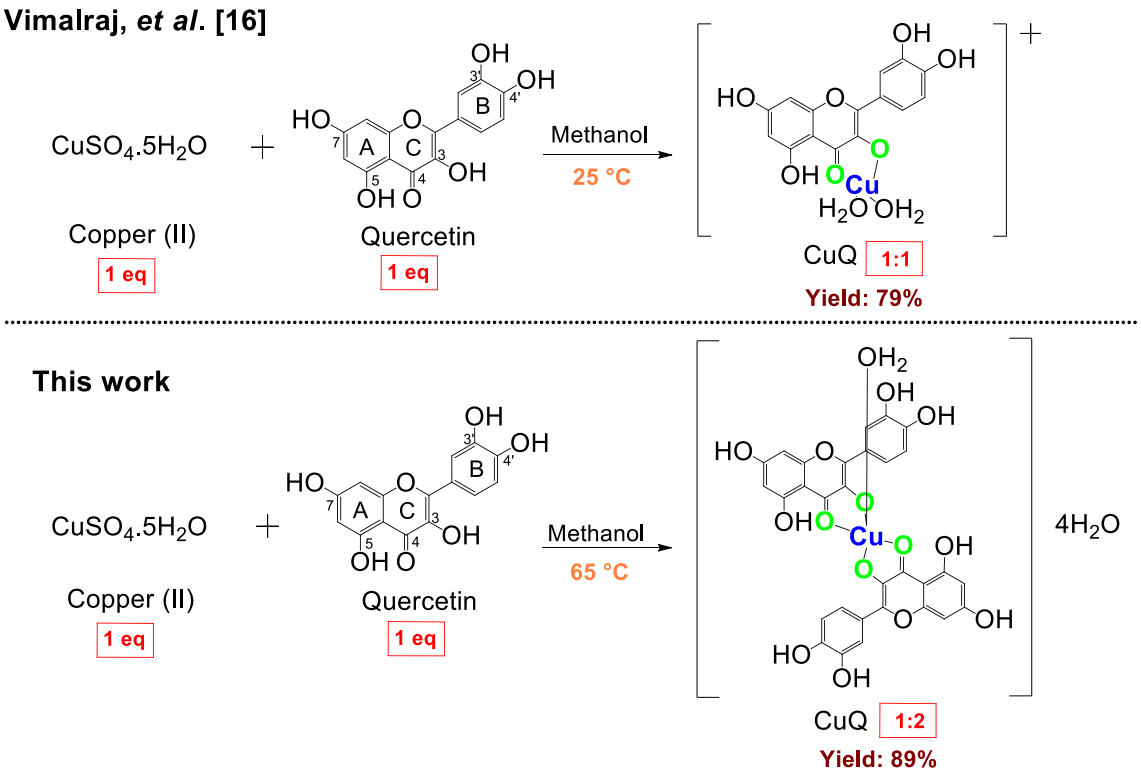

Figure 1. Temperature-dependent synthesis of Cu(II)–quercetin complexes in methanol [16].

Fenton-type systems under certain conditions [15]. Furthermore, Cu(II)-quercetin (CuQ) exhibits bioactivities relevant to osteogenic [16], angiogenic, antimicrobial [17], antitumor [18], and anticancer activities [10].

The reported stoichiometry of CuQ complexes is strongly dependent on synthesis conditions. In methanol at room temperature, Vimalraj et al. [16] reported a 1:1 CuQ complex, coordinated primarily through the 3-OH/4-oxo site. Under similar conditions, Sajid et al. [17] observed both 1:1 and 1:2 CuQ species. The outcome varied with the copper precursor ($CuCl_2$ or $CuSO_4$) and the Q source (pure Q or onion-peel extract), while maintaining the same dominant binding at the 3-OH/4-oxo site. Notably, the spectroscopic patterns were described as broadly comparable despite evident changes in complex color. Importantly, the 1:2 (Cu:Q) complex is generally more thermodynamically stable and exhibits higher antioxidant and antibacterial activities than the 1:1 form. In ethanol at room temperature, Muñoz et al. [19] also reported a 1:2 CuQ complex with 3-OH/4-oxo coordination, supported by the Yoe–Jones method and DFT calculations. The same study further showed that increasing the temperature (15–30 °C) promotes complex formation, consistent with its enhanced thermodynamic stability [19]. Consistent 1:2 stoichiometry has also been reported by Azeez et al. [13] and Jomova et al. [15] using Job's plot analysis, complemented by DFT (B3LYP), with an analogous coordination motif. In contrast, Bukhari et al. [20] proposed a possible 2:1 (Cu:Q) complex in methanol at room temperature, involving both the 3-OH/4-oxo and 5-OH/4-oxo sites.

This study investigates the influence of thermal conditions (65 °C) on the coordination environment and stoichiometry during CuQ complexation. The synthesis was carried out using an equimolar Cu (II):Q ratio (1:1) in methanol, following a modified procedure of Vimalraj et al. [16] (Figure 1). Under these conditions, the reaction predominantly yields the bis(Q) Cu(II) complex, $[Cu(H_2O)(Q)_2]\cdot 4H_2O$ (Cu:Q = 1:2), isolated in 89% yield. DFT calculations support the proposed binding mode (3-OH/4-oxo chelation) and indicate the relative stability of the 1:2 complex. The α-amylase inhibitory activities of the complex and free Q were then evaluated under identical assay conditions.

2. MATERIALS AND METHODS

2.1. Materials

Copper(II) sulfate pentahydrate ($CuSO_4 \times 5H_2O$), Q ($C_{15}H_{10}O_7$), and starch were purchased from Sigma-Aldrich Reagent, USA. Diethyl ether ($C_4H_{10}O$), enzyme pancreatin (8000 E/g amylase), ethanol (C_2H_5OH), iodine (I_2), methanol (CH_3OH), potassium iodide (KI), sodium dihydrogen phosphate dihydrate ($NaH_2PO_4 \cdot 2H_2O$), and disodium hydrogen phosphate (Na_2HPO_4) were purchased from Merck, Germany. Acarbose was purchased from OGB Dexa, Indonesia.

2.2. Methods

2.2.1. Synthesis of $[Cu(H_2O)(Q)_2] \cdot 4H_2O$

The synthesis method refers to the research by Vimalraj, et al. [16] with a complexation temperature of 65 °C. Q (0.5 mmol) was dissolved in 25 mL of methanol, followed by the addition of $CuSO_4 \cdot 5H_2O$ (0.5 mmol), yielding a dark brown solution. The mixture was heated to 65 °C under stirring for 1 h, then refrigerated for 3 days. The final product was filtered, washed with diethyl ether, dried in a vacuum desiccator, and recrystallized from methanol. Yield: 89%. Found: C, 47.44; H, 3.80; Cu, 8.40%. Analytical values for $C_{30}H_{28}CuO_{19}$: C, 47.61; H, 3.70; Cu, 8.40%.

2.2.2. Cu(II)-quercetin Characterization

The CuQ complex was characterized using various instrumental techniques. Electronic absorption and complex-formation features were examined by UV–Vis spectroscopy (UV-Vis, Shimadzu UV-188). Functional groups were examined by Fourier transform infrared spectroscopy (FTIR, PerkinElmer Spectrum 100). The proton environment of Q was analyzed by proton nuclear magnetic resonance (^{1}H NMR, JEOL ECZ-500R). Elemental composition (C, H, and N) was determined using an elemental analyzer (EA, Leco CHN628), while copper content was measured by an atomic absorption spectrophotometer (AAS, Shimadzu AA-700). Thermal stability and decomposition behavior were evaluated by thermogravimetric analysis (TGA, TGA 5500). Magnetic properties were determined using a magnetic susceptibility balance (MSB, Sherwood Scientific MSB). The α-amylase inhibitory activity was measured spectrophotometrically using a visible spectrophotometer (721G).

2.2.3. α-amylase Inhibition Assay

The α-amylase inhibitory activity was evaluated using a modified Fuwa method [3][21]. A 1000 µM stock solution of CuQ was prepared, centrifuged to remove insoluble material, and the supernatant was diluted to the desired concentrations. Pancreatin

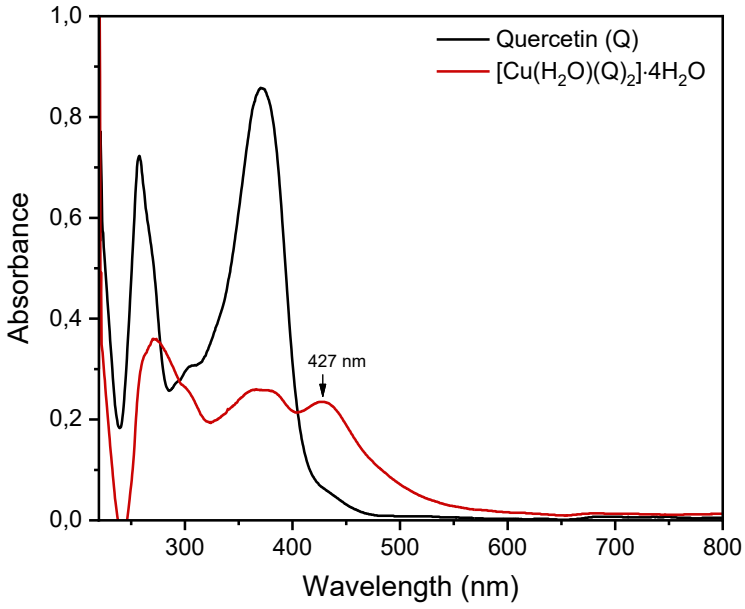

Figure 2. UV-Vis spectra of quercetin and $[Cu(H_2O)(Q)_2] \cdot 4H_2O$.

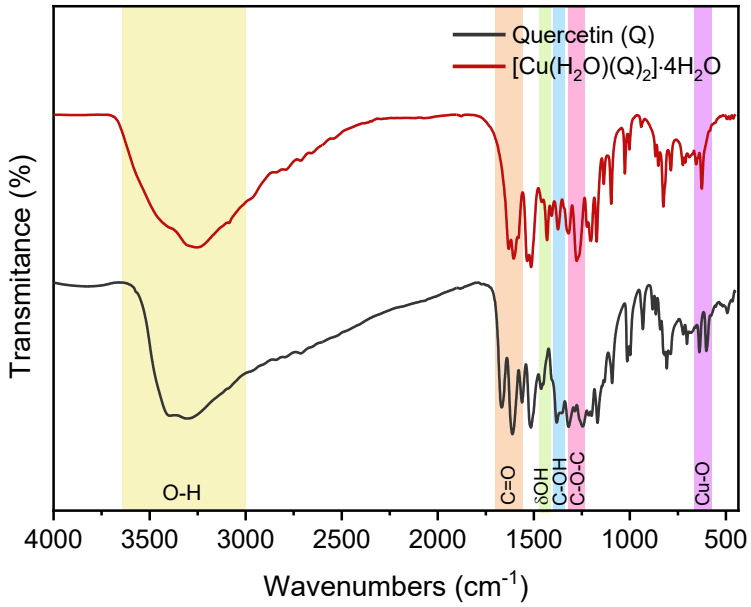

Figure 3. FTIR spectra of quercetin and $[Cu(H_2O)(Q)_2]\cdot 4H_2O$.

Table 1. Interpretation of absorption band data on FTIR spectra of quercetin and $[Cu(H_2O)(Q)_2]\cdot 4H_2O$.

Wavenumber (cm^{-1})		Functional group
Quercetin	**$[Cu(H_2O)(Q)_2]\cdot 4H_2O$**	
3306 [b]	3256 [b]	OH
1667 [s]	1631 [w]	C=O
1462 [w]	1431 [s]	δ OH
1381 [s]	1374 [s]	C–OH
1246 [s]	1277 [s]	C–O–C
-	626 [s]	Cu–O

b = broad; s = sharp; w = wide

was dissolved in sodium phosphate buffer (pH 6.9) to obtain a 50 ppm enzyme solution. Equal volumes (100 µL) of the complex solution and enzyme solution were incubated at 37 °C for 15 min. Subsequently, 100 µL of starch solution (0.1% w/v) was added, followed by further incubation for 10 min at 37 °C. The reaction was terminated by adding 0.1 N HCl (100 µL) and iodine solution. The mixture was then diluted with distilled water to a final volume of 2.0 mL, and the absorbance was measured at 600 nm using a visible spectrophotometer. All measurements were performed in triplicate. Free quercetin and acarbose were evaluated under identical conditions as positive controls. The percentage of α-amylase inhibition was calculated according to Jaishree and Narsimha [3] (Equation (1));

$$\text{Inhibition } (\%) = \frac{(A-B)-(C-D)}{(A-B)} \times 100\% \quad \textbf{(1)}$$

where A is the absorbance of the buffer with enzyme, B is the absorbance of the buffer alone, C is the absorbance of the sample solution with enzyme, and D is the absorbance of the sample solution in the buffer without enzyme.

2.2.4. DFT Computational Methods

All calculations were performed using Gaussian 09 Revision D.01 [22] at the SMD-M06/def2-TZVP//M06/def2-SVP level of theory [23]–[25] in implicit methanol, unless otherwise stated. Frequency calculations at the M06/def2-SVP level were performed to confirm that the optimized structures correspond to true minima—i.e., no imaginary (negative) frequencies were detected. Natural bond orbital (NBO) analysis was conducted using the NBO version integrated within Gaussian 09 Revision D.01 [26]. Visualization of computational results was conducted with GaussView 5.0.9 [27]. The reaction free energy

($\Delta G^{o}_{reaction}$) was calculated in methanol according to Equation (2).

$$\Delta G^{o}_{reaction} = \Sigma G^{o}_{product} - \Sigma G^{o}_{reactant} \quad (2)$$

For the formation of the $[Cu(Q)(H_2O)_2]^+$ complex, the $\Sigma G^{o}_{product}$ and $\Sigma G^{o}_{reactant}$ are expressed by Equations (3) and (4):

$$\Sigma G^{o}_{product} = G^{o}([Cu(Q)(H_2O)_2]^+) \quad (3)$$

$$\Sigma G^{o}_{reactant} = G^{o}(Cu^{2+}) + 2\times G^{o}(H_2O) + G^{o}(quercetin^-) \quad (4)$$

Meanwhile, for the formation of the $[Cu(H_2O)(Q)_2]$ complex, they are given by Equations (5) and (6):

$$\Sigma G^{o}_{product} = G^{o}([Cu(H_2O)(quercetin)_2]) \quad (5)$$

$$\Sigma G^{o}_{reactant} = G^{o}(Cu^{2+}) + G^{o}(H_2O) + 2\times G^{o}(quercetin^-) \quad (6)$$

3. RESULTS AND DISCUSSIONS

3.1. Synthesis and Composition of The Complex

The $[Cu(H_2O)(Q)_2]\cdot 4H_2O$ was prepared by heating Q with $CuSO_4\cdot 5H_2O$ in methanol at 65 °C for 1 h, yielding a brown-green solid in 89% yield. Elemental analysis and AAS gave C = 47.44, H = 3.80, and Cu = 8.40%, which are consistent with the calculated values for $C_{30}H_{28}CuO_{19}$ (C = 47.61, H = 3.70, Cu = 8.40%). Q was characterized by ^{1}H-NMR spectroscopy (500 MHz, DMSO-d_6): δ 12.48 (1H, *s*, 5-OH), 10.81 (1H, *s*, 7-OH), 9.62 (1H, *s*, 3-OH), 9.40 (1H, *s*, 4′-OH), 9.34 (1H, *s*, 3′-OH), 7.67 (1H, *d*, *J* = 2.20 Hz, H-2′), 7.54 (2.23 Hz, 1H, *dd*, *J* = 8.58, H-6′), 6.88 (1H, *d*, *J* = 8.45 Hz, H-5′), 6.40 (1H, *d*, *J* = 2.05 Hz, H-8), and 6.18 (1H, *d*, *J* = 2.0 Hz, H-6) (Figure S1). Due to its paramagnetic nature, the complex $[Cu(H_2O)(Q)_2]\cdot 4H_2O$ is not suitable for NMR analysis.

3.2. Spectroscopic Analysis

In the UV–Vis spectrum of Q, band II (A-ring benzoyl system) appears in the 250–300 nm region at λ_{max} = 257 nm. Band I (B-ring cinnamoyl system) is located in the 300–400 nm region, with a maximum at λ_{max} = 372 nm. Both bands arise primarily from π→π* transitions [12][19]. Upon coordination with Cu(II), band I shifts from 371 to 373 nm, while band II shifts from 257 to 271 nm. This bathochromic shift toward longer wavelengths indicates coordination of Cu(II) and possible ligand-to-metal charge transfer. These observations are consistent with previously reported bathochromic shifts associated with metal ion–flavonoid interactions [12][19]. The UV-Vis spectra of Q and the complex were recorded in ethanol (Figure 2). The experimental results are consistent with the DFT calculation (Figure S2 and Table S1).

The appearance of a new absorption band at 427 nm indicates the formation of a metal-flavonoid complex, as neither metal ion nor the free ligand

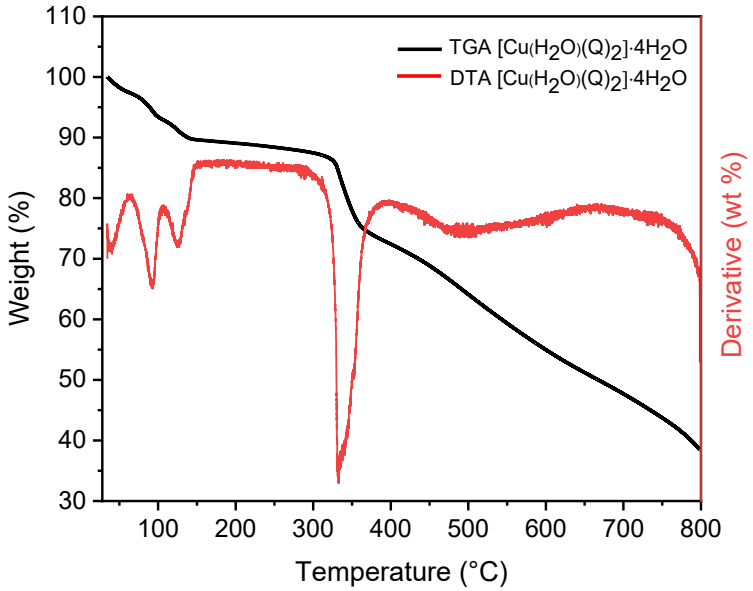

Figure 4. TGA-DTA spectrum of $[Cu(H_2O)(Q)_2]\cdot 4H_2O$.

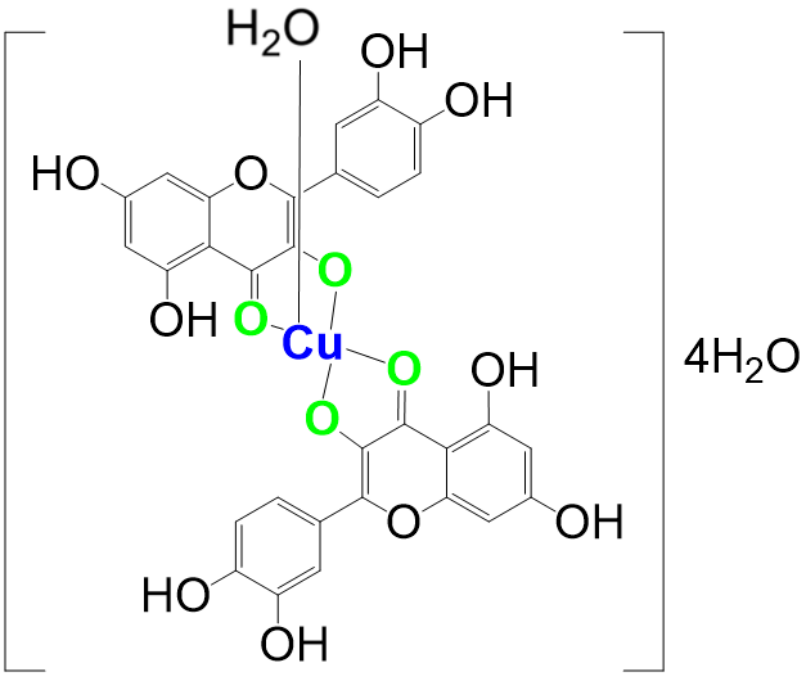

Figure 5. The $[Cu(H_2O)(Q)_2]\cdot 4H_2O$ proposed structure.

shows absorption at this wavelength [19][28]. The observed spectral changes upon addition of Cu(II) suggest that the electronic structure of Q is affected by metal coordination. These changes are consistent with the involvement of the cinnamoyl system and possible coordination through the 3-OH/4-oxo site, as reported in previous studies [13][29]. The 3-OH group, which contains the most acidic proton, is considered the primary site for complexation, typically involving the 3-OH/4-oxo chelation site. The 3′-4′-hydroxyl groups may act as secondary donors. In contrast, the 5-OH/4-oxo site is generally less involved due to the lower acidity and steric inaccessibility of the 5-OH [13][30]–[32].

Fourier transform infrared spectroscopy (FTIR) spectra of Q and CuQ were recorded in the range of 400–4000 cm^{-1} (Figure 3). The main absorption bands and their assignments are summarized in Table 1. For free Q, a strong band at 1667 cm^{-1} is attributed to the ν(C=O) stretching vibration of the 4-oxo group. In the spectrum of the CuQ complex, this band shifts to 1631 cm^{-1}, indicating a decrease in the C=O bond order upon coordination. This shift suggests the involvement of the C=O group, together with a neighboring phenolic hydroxyl group (3-OH or 5-OH), in chelation to Cu(II) [19][31].

In quercetin, a strong band at 1462 cm^{-1}, assigned to the δ(OH) bending mode, decreases significantly upon complexation, suggesting the involvement of the phenolic OH group in metal coordination [19]. The spectra show bands at 1381 cm^{-1} for free Q and 1374 cm^{-1} for $[Cu(H_2O)(Q)_2]\cdot 4H_2O$, corresponding to ν(C–OH) vibrations. These observations indicate that coordination alters the phenolic environment [16]. The characteristic ν (C–O–C) of the complex appears at 1262 cm^{-1}, shifted from 1246 cm^{-1} in free Q, suggesting an increase in bond order upon coordination [33].

The broad band at 3306 cm^{-1} in free Q is attributed to O–H stretching, associated with hydrogen bonding of phenolic groups. In the complex, this band shifts to 3256 cm^{-1}, indicating changes in hydrogen bonding and/or partial deprotonation of phenolic O–H groups [16], possibly due to the presence of lattice- or coordinated water molecules [34], consistent with EA data. Additionally, a new band at 626 cm^{-1} appears in the complex spectrum and is assigned to Cu–O stretching, which is absent in the free ligand [13][16][19]. Metal–oxygen stretching vibrations, ν (M–O), are typically observed in the 410–590 cm^{-1} region [13], providing further evidence for the formation of a Cu–O bond between the metal center and Q oxygen donors [16][19].

3.3. Thermal Analysis

Thermogravimetric-differential thermal analysis (TGA-DTA) (Figure 4) reveals the dehydration and decomposition of the complex. The first weight loss occurs between 30–140 °C, with an observed loss of 10.06% (calculated 9.52%), corresponding to the release of four uncoordinated water molecules. This assignment is consistent with previous reports showing that uncoordinated water is typically released in the 90–140 °C range [35]. The second weight loss, measured at 140–365 °C (14.64% observed, 14.42% calculated), is attributed to the initial or partial thermal decomposition of the organic ligand framework. EA and FTIR data further support the presence of water molecules in the complex, consistent with the proposed formulation. The FTIR spectrum of the CuQ exhibits a broad band at 3256 cm^{-1}, assigned to O–H stretching vibrations of water molecules, corresponding to water of crystallization [34].

3.4. Structure of Complex

The observed magnetic moment (μ_{eff} = 1.79 BM at 298 K) indicates that the complex is paramagnetic and is consistent with a mononuclear Cu(II) center possessing one unpaired electron ($3d^9$ configuration) [36]. This value falls within the typical range reported for Cu(II) complexes (1.7–2.2 BM). According to Kato et al. [37], magnetic moments in the range of 1.72–1.82 BM suggest increased covalent character. The proposed structure (Figure 5**)** is supported by EA, TGA-DTA, UV-Vis, FTIR, and MSB data, corresponding to the formulation $[Cu(H_2O)(Q)_2]\cdot 4H_2O$ ($C_{30}H_{28}CuO_{19}$).

The characterization results suggest the formation of a CuQ complex with a 1:2 stoichiometry. The data are consistent with coordination through the 3-OH/4-oxo chelation site, in agreement with previous studies. Lekka et al. [38] reported that coordination of Cu(II) with two 3 -OH/4-oxo chelate sites from two quercetin

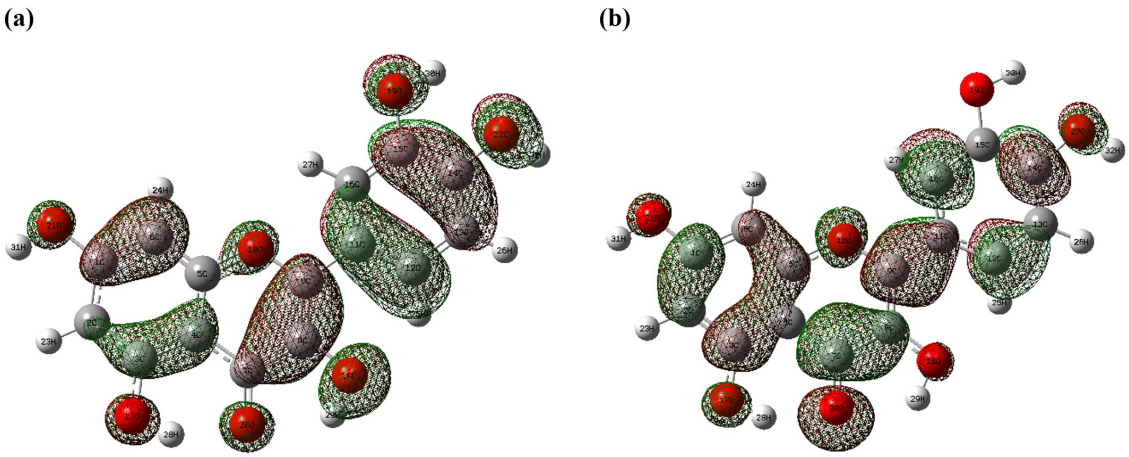

Figure 6. The (a) HOMO and (b) LUMO of quercetin in methanol at the SMD-M06/def2-TZVP//M06/ def2-TZVP level of theory.

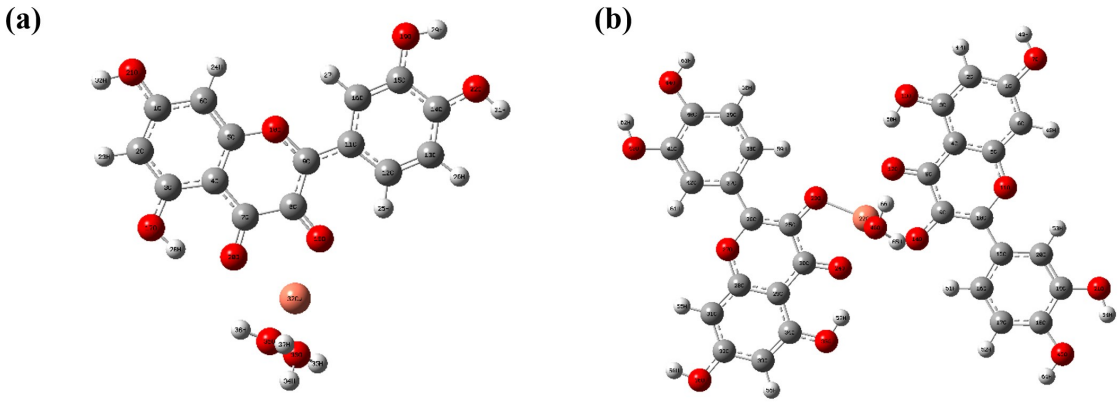

Figure 7. The optimized structure of (a) $[Cu(Q)(H_2O)_2]^+$ and (b) $[Cu(H_2O)(Q)_2]$.

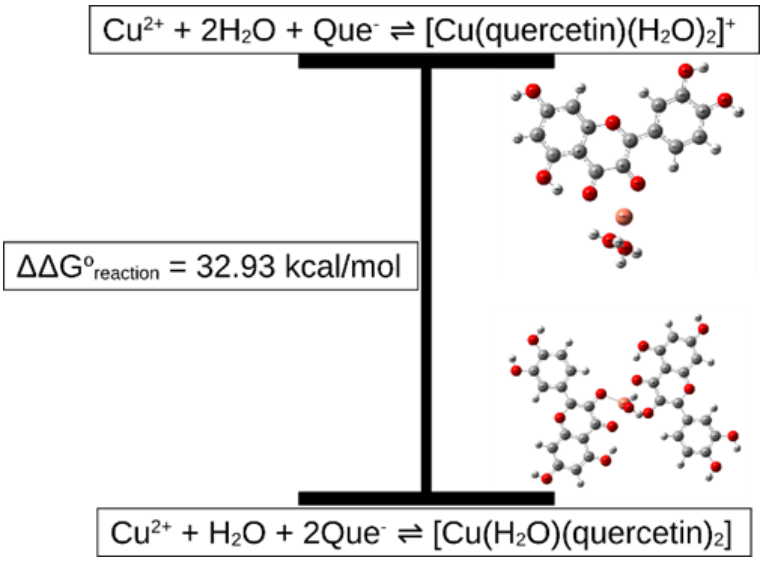

Figure 8. Comparison of 1:1 and 1:2 CuQ complex formation pathways with corresponding ΔΔG° values.

molecules provides optimal orbital overlap and minimal steric hindrance, resulting in the lowest total energy among possible coordination modes, such as 5-OH/4-oxo chelation. Muñoz et al. [19] further showed that CuQ complexation is endothermic ($\Delta H > 0$), with positive ΔS and negative ΔG, indicating enhanced complex stability at higher temperatures. DFT calculations also support that the 3-OH/4-oxo site is the most favorable binding site for Cu(II), consistent with the experimental results [19].

The reaction conducted at 65 °C favors the formation of more thermodynamically stable CuQ species by facilitating ligand reorganization. In general, kinetic products form rapidly via lower activation barriers, whereas thermodynamic products correspond to more stable configurations favored at elevated temperatures and longer reaction times [39]. Chen et al. [8] demonstrated that increasing the synthesis temperature from 22 to 60 °C enhances the extent of CuQ complexation in a liposomal system without disrupting vesicle structure, highlighting temperature as a key parameter in complex formation. In this context, higher temperatures may favor the formation of more stable metal–ligand assemblies, such as the 1:2 Cu(II):Q complex [19]. These findings support the role of temperature in determining whether kinetic or thermodynamic pathways dominate during complex formation and crystallization [39], in agreement with the spectroscopic and computational results obtained in this study.

3.5. DFT Computational Results

The dipole moment vector of Q (Figure S4) suggests that the negative dipole is oriented toward the region around the 5-OH and 4-oxo sites. Electron population analysis shows that the partial charge on the 4-oxo oxygen atom is the most negative (Table S2), suggesting that this site may serve as the initial interaction site for Cu^{2+}. The optimized structure of Q is presented in Figure S2.

The HOMO of Q is delocalized over all oxygen atoms (Figure 6). However, analysis of atomic orbital contributions indicates that the 3-OH site contributes the most, suggesting it acts as the primary nucleophilic site (Table S3). These results suggest that interaction between Cu^{2+} and the 4-oxo group may initiate complex formation, followed by electron donation from the 3-OH oxygen to the metal center.

The optimized structures of the $[Cu(Q)(H_2O)_2]^+$ and $[Cu(H_2O)(Q)_2]$ are shown in Figure 7. The $[Cu(Q)(H_2O)_2]^+$ complex adopts a distorted tetrahedral geometry, whereas $[Cu(H_2O)(Q)_2]$ exhibits a square-pyramidal geometry. This distorted tetrahedral arrangement is consistent with previous reports showing that hydrated Cu^{2+} species can display mixed tetrahedral, trigonal-bipyramidal, and distorted octahedral geometries [40]. The calculated charge distribution of hydroxyl hydrogen atoms in Q is summarized in Table S4, while the corresponding Wiberg bond indices (WBI) are presented in Table S5.

The calculated reaction free energies for CuQ

complex formation in methanol suggest that the 1:2 complex, $[Cu(H_2O)(Q)_2]$, is predicted to be more stable than the 1:1 species, $[Cu(Q)(H_2O)_2]^+$, in agreement with the experimental observations at 65 °C (Figure 1). The relative reaction free energy difference ($\Delta\Delta G°_{reaction}$) represents the Gibbs free energy difference between the 1:1 and 1:2 complexes. A value of 32.93 kcal mol^{-1} indicates a clear energetic preference for the 1:2 complex (Figure 8). Analysis of the O_{ipso}–Cu bond distances and WBI shows that the interaction between Cu and Q is stronger in $[Cu(H_2O)(Q)_2]$ than in $[Cu(Q)(H_2O)_2]^+$. However, coordination of two bulky Q ligands to Cu^{2+} requires overcoming additional kinetic barriers associated with ligand–ligand exchange repulsion during formation of the coordination covalent bonds [41][42]. This may explain the requirement for elevated temperature (65 °C) in the present study.

In both complexes, the Cu–O_{ipso} bond distances involving the 3-OH group are shorter than those involving the 4-oxo oxygen (Table S6 and Table S7). In addition, the O_{ipso}–Cu WBI for the 3-OH are higher than for the 4-oxo oxygen, suggesting a stronger interaction between Cu^{2+} and the 3-OH (Table S8 and Table S9).

3.6. α-Amylase Inhibitory Activity

The α-amylase inhibitory activity of $[Cu(H_2O)(Q)_2]\cdot 4H_2O$ was evaluated using the Fuwa starch–iodine assay at 600 nm (pH 6.9, 37 °C), alongside free Q and acarbose (Figure 9). All measurements were performed in triplicate, and the results are expressed as mean ± standard deviation; error bars in Figure 9 represent the standard deviation of the measurements. Across the tested concentration range, $[Cu(H_2O)(Q)_2]\cdot 4H_2O$ exhibited higher percentage inhibition than Q, with apparent IC_{50} values of 450 µM (Q), 133 µM (CuQ), and 148 µM (acarbose), calculated after blank correction according to Equation (1). These results demonstrate that Cu(II) coordination enhances the α-amylase inhibitory activity of Q under the present conditions. The reported IC_{50} values represent apparent estimates obtained under identical assay conditions and are intended for comparative evaluation. While the results demonstrate reproducible α-amylase inhibition, the biological assessment is currently based on a single colorimetric assay. Further studies are therefore required to elucidate the underlying mechanism of inhibition.

Flavonoids inhibit α-amylase through a combination of hydrogen bonding and hydrophobic interactions near the catalytic region (Asp197, Glu233, and Asp300) and adjacent binding pockets. These interactions may interfere with substrate binding at or near the active site, thereby reducing

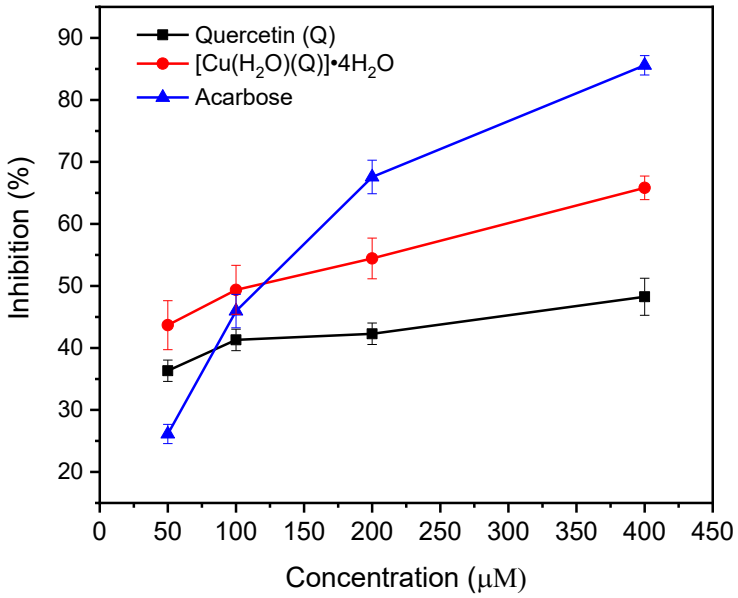

Figure 9. Inhibitory activity of α-amylase enzyme by quercetin, $[Cu(H_2O)(Q)_2]\cdot 4H_2O$, and acarbose. Data represent the mean ± SD of three replicates (n = 3); error bars indicate standard deviation (SD).

enzyme activity. The molecular structure of flavonoids, including hydroxyl groups, conjugated double bonds, and structural planarity, significantly impacts binding affinity and inhibitory activity [43].

Q has been reported to act as a mixed inhibitor [43] or a non-competitive inhibitor [44] depending on experimental conditions. Structure–activity studies further highlight the importance of hydroxyl groups at C5/C7 (ring A) and C3′/C4′ (ring B), as well as the C2=C3 double bond, in determining inhibitory potency [43][45]. Coordination to Cu(II) preserves these key structural features and may contribute to the improved apparent potency compared to free Q. The presence of Cu(II) may enhance interactions with the enzyme through hydrogen bonding and metal coordination with catalytic residues, thereby influencing inhibitory activity [6]. These effects may be associated with changes in electronic structure and molecular orientation upon complexation. However, further studies, such as enzyme kinetics or molecular docking, are required to clarify the detailed mechanism of inhibition.

4. CONCLUSIONS

The $[Cu(H_2O)(Q)_2]\cdot 4H_2O$ complex was successfully synthesized in 89% yield from an equimolar Cu(II):Q (1:1) ratio in methanol at 65 °C. EA, AAS, UV–Vis, FTIR, thermal, and magnetic data support the formation of a mononuclear Cu(II) complex with a 1:2 metal–ligand stoichiometry. The spectroscopic and computational results are consistent with coordination via the 3-OH/4-oxo donor sites, with one coordinated water molecule and four lattice water molecules. Compared to room -temperature conditions that favor kinetically formed mono(quercetin) complexes, elevated temperature (65 °C) promotes the formation of the 1:2 complex. DFT calculations in implicit methanol indicate a relative thermodynamic preference for the 1:2 complex over the 1:1 species ($\Delta\Delta G^{o}_{reaction}$ = 32.93 kcal mol^{-1}), consistent with the experimental observations. The complex exhibits enhanced α-amylase inhibitory activity (IC_{50} = 133 µM) compared to free Q (IC_{50} = 450 µM), with an apparent IC_{50} value falling within the same concentration range as acarbose under identical assay conditions. These results suggest that Cu(II) coordination may enhance the inhibitory activity of Q under the present experimental conditions. Overall, temperature-controlled complexation with Cu(II) influences the structural properties of the complex and is associated with enhanced *in vitro* α-amylase inhibitory activity. These results provide a basis for further mechanistic studies of metal–flavonoid systems.

AUTHOR INFORMATION

Corresponding Author

Yudha Prawira Budiman — Department of Chemistry, Padjadjaran University, Sumedang-45363 (Indonesia);
orcid.org/0000-0002-3929-1891
Email: y.p.budiman@unpad.ac.id

Authors

Puteri Khansa Salsabila — Department of Chemistry, Padjadjaran University, Sumedang-45363 (Indonesia);
orcid.org/0009-0005-0455-0469

Yusi Deawati — Department of Chemistry, Padjadjaran University, Sumedang-45363 (Indonesia);
orcid.org/0000-0002-4561-8715

Regaputra Satria Janitra — Department of Chemistry, Padjadjaran University, Sumedang-45363 (Indonesia);
orcid.org/0000-0003-2073-8849

Safri Ishmayana — Department of Chemistry, Padjadjaran University, Sumedang-45363 (Indonesia);
orcid.org/0000-0002-9825-4425

Iman Permana Maksum — Department of Chemistry, Padjadjaran University, Sumedang-45363 (Indonesia);
orcid.org/0000-0001-8166-8421

Yessi Permana — Division of Inorganic and Physical Chemistry, Institut Teknologi Bandung, Bandung-40132 (Indonesia);
orcid.org/0000-0002-1553-7105

Author Contributions

Conceptualization, P. K. S., Y. D., and Y. P. B.; Methodology, P. K. S., Y. D., R. S. J., Y. P. B., and S. I.; Software, R. S. J.; Validation, Y. D., Y. P. B., S. I., I. P. M., and Y. P.; Formal Analysis, P. K. S.,

Y. D., R. S. J., and Y. P. B.; Investigation, P. K. S., Y. D., and R. S. J.; Resources, Y. D. and S. I.; Data Curation, P. K. S., Y. D., and R. S. J.; Writing – Original Draft Preparation, P. K. S., Y. D., R. S. J., and Y. P. B.; Writing – Review & Editing, P. K. S., Y. D., R. S. J., Y. P. B., and Y. P.; Visualization, P. K. S. and R. S. J.; Supervision, Y. D., Y. P. B., S. I., I. P. M., and Y. P.; Project Administration, Y. D. and Y. P. B.; Funding Acquisition, I. P. M. and Y. P. B.

Conflicts of Interest

The authors declare no conflict of interest.

SUPPORTING INFORMATION

Supplementary data associated with this article can be found in the online version at doi: 10.47352/jmans.2774-3047.383

ACKNOWLEDGEMENT

Y. P. B. acknowledges financial support from Universitas Padjadjaran for a Competency Research Grant for Lecturers at Universitas Padjadjaran (RKDU, 2025). Y. D. acknowledges the Directorate General of Higher Education, the Ministry of Research and Technology of Indonesian Republic, for the PFR research fund (contract number: 148/E5/PG.02.00.PL/2023 in June 19th, 2023) and the Universitas Padjadjaran for the Academic Leadership Grant in 2023 (contract number: 1549/UN6.3.1/PT.00/2023 in March 27th, 2023) as a financial support provider for the continuation of this research.

DECLARATION OF GENERATIVE AI

AI was not involved in the generation or manipulation of scientific data, figures, results, or conclusions.

REFERENCES

[1] R. Q. Xiang, Y. F. Niu, J. Han, Y. L. Lau, H. H. Wu, and X. L. Zhao. (2019). "A Neutral Cu-Based MOF for Effective Quercetin Extraction and Conversion from Natural Onion Juice". *RSC Advances.* **9** (58): 33716-33721. 10.1039/C9RA04551A.

[2] J. Mlcek, T. Jurikova, S. Skrovankova, and J. Sochor. (2016). "Quercetin and Its Anti-Allergic Immune Response". *Molecules.* **21** (5): 623. 10.3390/molecules21050623.

[3] V. Jaishree and S. Narsimha. (2020). "Swertiamarin and Quercetin Combination Ameliorates Hyperglycemia, Hyperlipidemia and Oxidative Stress in Streptozotocin-Induced Type 2 Diabetes Mellitus in Wistar Rats". *Biomedicine & Pharmacotherapy.* **130** : 110561. 10.1016/j.biopha.2020.110561.

[4] S. Oliver, E. Yee, M. Kavallaris, O. Vittorio, and C. Boyer. (2018). "Water Soluble Antioxidant Dextran-Quercetin Conjugate with Potential Anticancer Properties". *Macromolecular Bioscience.* **18** (4): 1700239. 10.1002/mabi.201700239.

[5] M. Azeem, M. Hanif, K. Mahmood, N. Ameer, F. R. S. Chughtai, and U. Abid. (2023). "An Insight into Anticancer, Antioxidant, Antimicrobial, Antidiabetic and Anti-Inflammatory Effects of Quercetin: A Review". *Polymer Bulletin.* **80** : 241-262. 10.1007/s00289-022-04091-8.

[6] B. K. Raut, S. R. Upadhyaya, J. Bashyal, and N. Parajuli. (2023). "In Silico and In Vitro Analyses to Repurpose Quercetin as a Human Pancreatic Alpha-Amylase Inhibitor". *ACS Omega.* **8** : 43617-43631. 10.1021/acsomega.3c05082.

[7] P. Mukhopadhyay and A. K. Prajapati. (2015). "Quercetin in Anti-Diabetic Research and Strategies for Improved Quercetin Bioavailability Using Polymer-Based Carriers: A Review". *RSC Advances.* **5** (118): 97547-97562. 10.1039/C5RA18896B.

[8] K. T. J. Chen, M. Anantha, A. W. Y. Leung, J. A. Kulkarni, G. G. C. Militao, M. Wehbe, B. Sutherland, P. R. Cullis, and M. B. Bally. (2020). "Characterization of a Liposomal Copper(II)-Quercetin Formulation Suitable for Parenteral Use". *Drug Delivery and Translational Research.* **10** (1): 202-215. 10.1007/s13346-019-00674-7.

[9] D. Xu, M. J. Hu, Y. Q. Wang, and Y. L. Cui. (2019). "Antioxidant Activities of Quercetin and Its Complexes for Medicinal Application". *Molecules.* **24** (6): 1123.

10.3390/molecules24061123.

[10] H. Mutlu Gençkal, M. Erkisa, P. Alper, S. Sahin, E. Ulukaya, and F. Ari. (2019). "Mixed Ligand Complexes of Co(II), Ni(II) and Cu(II) with Quercetin and Diimine Ligands: Synthesis, Characterization, Anti-Cancer and Anti-Oxidant Activity". *Journal of Biological Inorganic Chemistry.* **25** (1): 161-177. 10.1007/s00775-019-01749-z.

[11] T. S. de Castilho, T. B. Matias, K. P. Nicolini, and J. Nicolini. (2018). "Study of Interaction Between Metal Ions and Quercetin". *Food Science and Human Wellness.* **7** (3): 215-219. 10.1016/j.fshw.2018.08.001.

[12] W. M. B. da Silva, S. de Oliveira Pinheiro, D. R. Alves, J. E. S. A. de Menezes, F. E. A. Magalhães, F. C. O. Silva, J. Silva, E. S. Marinho, and S. M. de Morais. (2020). "Synthesis of Quercetin-Metal Complexes, In Vitro and In Silico Anticholinesterase and Antioxidant Evaluation, and In Vivo Toxicological and Anxiolytic Activities". *Neurotoxicity Research.* **37** : 893-903. 10.1007/s12640-019-00142-7.

[13] L. Azeez, A. O. Oyedeji, S. O. Adewuyi, and K. O. Tijani. (2015). "Syntheses, Characterizations and Antioxidant Activities of Copper Complexes of Quercetin as Influenced by Redox States". *International Journal of Biological and Chemical Sciences.* **9** (5): 2712-2718. 10.4314/ijbcs.v9i5.40.

[14] M. Kalinowska, G. Swiderski, M. Matejczyk, and W. Lewandowski. (2016). "Spectroscopic, Thermogravimetric and Biological Studies of Na(I), Ni(II) and Zn(II) Complexes of Quercetin". *Journal of Thermal Analysis and Calorimetry.* **126** : 141 -148. 10.1007/s10973-016-5362-5.

[15] K. Jomova, M. Lawson, L. Drostinova, P. Lauro, P. Poprac, V. Brezova, M. Michalik, V. Lukes, and M. Valko. (2017). "Protective Role of Quercetin Against Copper(II)-Induced Oxidative Stress: A Spectroscopic, Theoretical and DNA Damage Study". *Food and Chemical Toxicology.* **110** : 340-350. 10.1016/j.fct.2017.10.042.

[16] S. Vimalraj, S. Rajalakshmi, D. R. Preeth, S. V. Kumar, T. Deepak, V. Gopinath, K. Murugan, and S. Chatterjee. (2018). "Mixed-Ligand Copper(II) Complex of Quercetin Regulates Osteogenesis and Angiogenesis". *Materials Science and Engineering C.* **83** : 187-194. 10.1016/j.msec.2017.09.005.

[17] S. Sajid, N. Jahan, Z. Huma, M. I. Ali, A. Zada, A. Ibrar, G. A. Ashraf, L. Noureen, M. Ayaz, S. Arain, and F. Saeed. (2024). "Fabrication, Characterization, and In Vitro Testing of Nanostructured Systems". *Nano Biomedicine and Engineering.* **16** (3): 402-415. 10.26599/NBE.2024.9290085.

[18] J. Tan, B. Wang, and L. Zhu. (2009). "DNA Binding and Oxidative DNA Damage Induced by a Quercetin Copper(II) Complex: Potential Mechanism of Its Antitumor Properties". *Journal of Biological Inorganic Chemistry.* **14** (5): 727-739. 10.1007/s00775-009-0486-8.

[19] V. A. Muñoz, G. V. Ferrari, M. I. Sancho, and M. P. Montaña. (2016). "Spectroscopic and Thermodynamic Study of Chrysin and Quercetin Complexes with Cu(II)". *Journal of Chemical and Engineering Data.* **61** (2): 987-995. 10.1021/acs.jced.5b00837.

[20] S. B. Bukhari, S. Memon, M. Mahroof-Tahir, and M. I. Bhanger. (2009). "Synthesis, Characterization and Antioxidant Activity of Copper-Quercetin Complex". *Spectrochimica Acta Part A: Molecular And Biomolecular Spectroscopy.* **71** (5): 1901-1906. 10.1016/j.saa.2008.07.030.

[21] H. Fuwa. (1954). "A New Method for Microdetermination of Amylase Activity by the Use of Amylose as the Substrate". *Journal of Biochemistry.* **41** (5): 583-603. 10.1093/oxfordjournals.jbchem.a126476.

[22] M. J. Frisch, G. W. Trucks, H. B. Schlegel, G. E. Scuseria, M. A. Robb, J. R. Cheeseman, G. Scalmani, V. Barone, B. Mennucci, and G. A. Petersson. (2013). "Gaussian 09, Revision D.01". USA: Gaussian, Inc.

[23] A. V. Marenich, C. J. Cramer, and D. G. Truhlar. (2009). "Universal Solvation Model Based on Solute Electron Density and on a Continuum Model of the Solvent Defined by the Bulk Dielectric Constant and Atomic Surface Tensions". *Journal of Physical*

Chemistry B. **113** (18): 6378-6396. 10.1021/jp810292n.

[24] F. Weigend. (2006). "Accurate Coulomb-Fitting Basis Sets for H to Rn". *Physical Chemistry Chemical Physics.* **8** : 1057-1065. 10.1039/b515623h.

[25] F. Weigend and R. Ahlrichs. (2005). "Balanced Basis Sets of Split Valence, Triple Zeta Valence and Quadruple Zeta Valence Quality for H to Rn: Design and Assessment of Accuracy". *Physical Chemistry Chemical Physics.* **7** : 3297-3305. 10.1039/b508541a.

[26] E. D. Glendening, J. K. Badenhoop, A. E. Reed, J. E. Carpenter, J. A. Bohmann, C. M. Morales, and F. Weinhold. (2001). "NBO 3.1". USA: Theoretical Chemistry Institute, University of Wisconsin.

[27] R. Dennington, T. A. Keith, and J. M. Millam. (2008). "GaussView, Version 5". USA: Semichem Inc.

[28] A. Pękal, M. Biesaga, and K. Pyrzynska. (2011). "Interaction of Quercetin with Copper Ions: Complexation, Oxidation and Reactivity Towards Radicals". *BioMetals.* **24** (1): 41-49. 10.1007/s10534-010-9372-7.

[29] M. Samsonowicz and E. Regulska. (2017). "Spectroscopic Study of Molecular Structure, Antioxidant Activity and Biological Effects of Metal Hydroxyflavonol Complexes". *Spectrochimica Acta Part A: Molecular And Biomolecular Spectroscopy.* **173** : 757-771. 10.1016/j.saa.2016.10.031.

[30] E. Jabeen, N. K. Janjua, S. Ahmed, I. Murtaza, T. Ali, N. Masood, A. S. Rizvi, and G. Murtaza. (2017). "DFT Predictions, Synthesis, Stoichiometric Structures and Anti -Diabetic Activity of Cu(II) and Fe(III) Complexes of Quercetin, Morin, and Primuletin". *Journal of Molecular Structure.* **1150** : 459-468. 10.1016/j.molstruc.2017.09.003.

[31] S. Yang, B. Yin, L. Xu, B. Gao, H. Sun, L. Du, Y. Tang, W. Jiang, and F. Cao. (2015). "A Natural Quercetin-Based Fluorescent Sensor for Highly Sensitive and Selective Detection of Copper Ions". *Analytical Methods.* **7** (11): 4546-4551. 10.1039/C5AY00375J.

[32] G. A. Corrente, L. Malacaria, A. Beneduci, E. Furia, T. Marino, and G. Mazzone. (2021). "Experimental and Theoretical Study on the Coordination Properties of Quercetin Towards Aluminum(III), Iron(III) and Copper(II) in Aqueous Solution". *Journal of Molecular Liquids.* **325** : 115171. 10.1016/j.molliq.2020.115171.

[33] E. Halevas, A. Pekou, R. Papi, B. Mavroidi, A. G. Hatzidimitriou, G. Zahariou, G. Litsardakis, M. Sagnou, M. Pelecanou, and A. A. Pantazaki. (2020). "Synthesis, Physicochemical Characterization and Biological Properties of Two Novel Cu(II) Complexes Based on Natural Products Curcumin and Quercetin". *Journal of Inorganic Biochemistry.* **208** : 111083. 10.1016/j.jinorgbio.2020.111083.

[34] M. J. Afshar, Z. M. Nazari, and M. Chaichi. (2021). "Synthesis, Characterization, Antioxidant Studies and Scavenger Effect of Quercetin and Its Copper(II) Complexes on Hydrogen Peroxide-Induced Luminol Chemiluminescence". *Inorganic Chemistry Research.* **5** (1): 132-148. 10.22036/icr.2021.257885.1095.

[35] L. Tabrizi, D. Q. Dao, and T. A. Vu. (2019). "Experimental and Theoretical Evaluation on the Antioxidant Activity of a Copper(II) Complex Based on Lidocaine and Ibuprofen Amide-Phenanthroline Agents". *RSC Advances.* **9** (6): 3320-3335. 10.1039/C8RA09763A.

[36] M. M. Ibrahim, A. E. M. M. Ramadan, S. Y. Shaban, G. A. M. Mersal, S. A. El-Shazly, and S. Al-Juaid. (2017). "Syntheses, Characterization and Antioxidant Activity Studies of Mixed-Ligand Copper(II) Complexes of 2,2′-Bipyridine and Glycine: The X-Ray Crystal Structure of [Cu(BPy)(Gly)]ClO4". *Journal of Molecular Structure.* **1134** : 319-329. 10.1016/j.molstruc.2016.12.087.

[37] M. Kato, H. B. Jonassen, and J. C. Fanning. (1964). "Copper(II) Complexes with Subnormal Magnetic Moments". *Chemical Reviews.* **64** (2): 99-128. 10.1021/cr60228a003.

[38] C. E. Lekka, J. Ren, S. Meng, and E. Kaxiras. (2009). "Structural, Electronic, and Optical

Properties of Representative Cu-Flavonoid Complexes". *Journal of Physical Chemistry B.* **113** (18): 6478-6483. 10.1021/jp807948z.

[39] A. K. Cheetham and G. Kieslich. (2018). "Thermodynamic and Kinetic Effects in the Crystallization of Metal–Organic Frameworks". *Accounts of Chemical Research.* **51** : 659-667. 10.1021/acs.accounts.7b00497.

[40] D. T. Bowron, M. Amboage, R. Boada, A. Freeman, S. Hayama, and S. Díaz-Moreno. (2013). "The Hydration Structure of Cu2+: More Tetrahedral than Octahedral?". *RSC Advances.* **3** (39): 17803-17812. 10.1039/c3ra42400f.

[41] D. G. Fedorov. (2020). "Analyzing Interactions with the Fragment Molecular Orbital Method". *Methods in Molecular Biology.* **2114**. 10.1007/978-1-0716-0282-9_4.

[42] A. Heifetz, T. James, M. Southey, I. Morao, D. G. Fedorov, M. J. Bodkin, and A. Townsend-Nicholson. (2020). "Analyzing GPCR-Ligand Interactions with Fragment Molecular Orbital (FMO)". *Methods in Molecular Biology.* **2114** : 163-175. 10.1007/978-1-0716-0282-9_11.

[43] A. I. Martinez-Gonzalez, Á. G. Díaz-Sánchez, I. Bustos-Jaimes, and E. Alvarez-Parrilla. (2019). "Inhibition of α-Amylase by Flavonoids: Structure–Activity Relationship (SAR)". *Spectrochimica Acta Part A: Molecular And Biomolecular Spectroscopy.* **206** : 437-447. 10.1016/j.saa.2018.08.057.

[44] G. Oboh, A. O. Ademosun, P. O. Ayeni, O. S. Omojokun, and F. Bello. (2015). "Comparative Effect of Quercetin and Rutin on α-Amylase, α-Glucosidase, and Some Pro-Oxidant-Induced Lipid Peroxidation in Rat Pancreas". *Comparative Clinical Pathology.* **24** (5): 1103-1110. 10.1007/s00580-014-2040-5.

[45] C. Proença, M. Freitas, D. Ribeiro, S. M. Tomé, E. F. T. Oliveira, M. F. Viegas, A. N. Araújo, M. J. Ramos, A. M. S. Silva, P. A. Fernandes, and E. Fernandes. (2019). "Evaluation of a Flavonoids Library for Inhibition of Pancreatic α-Amylase Towards a Structure–Activity Relationship". *Journal of Enzyme Inhibition and Medicinal Chemistry.* **34** (1): 577-588. 10.1080/14756366.2018.1558221.